NASA TECHNICAL NOTE

NASA TN D-2773

X-RAY SPECTRA PRODUCED WHEN THICK SILICON TARGETS ARE BOMBARDED WITH 1.05 AND 1.25 MILLION VOLTS ELECTRONS

by Jag J. Singh, Richard Adams, and Chris Gross

Langley Research Center
Langley Station, Hampton, Va.

NATIONAL AERONAUTICS AND SPACE ADMINISTRATION • WASHINGTON, D. C. • DECEMBER 1966

NASA TN D-2773

X-RAY SPECTRA PRODUCED WHEN THICK SILICON TARGETS ARE BOMBARDED WITH 1.05 AND 1.25 MILLION VOLTS ELECTRONS

By Jag J. Singh, Richard Adams, and Chris Gross

Langley Research Center
Langley Station, Hampton, Va.

NATIONAL AERONAUTICS AND SPACE ADMINISTRATION

For sale by the Clearinghouse for Federal Scientific and Technical Information
Springfield, Virginia 22151 – Price $2.00

X-RAY SPECTRA PRODUCED WHEN THICK SILICON TARGETS ARE BOMBARDED WITH 1.05 AND 1.25 MILLION VOLTS ELECTRONS

By Jag J. Singh, Richard Adams,
and Chris Gross
Langley Research Center

SUMMARY

Measurements have been made on the X-rays produced when thick silicon targets are bombarded with 1.05 MeV and 1.25 MeV electrons. (These energies are based on range-energy relationship for electrons in aluminum.) The various cross sections, after correction for efficiency and finite resolution of the sodium iodide crystal for X-rays, have been compared with the predictions of the Bethe-Heitler theory. The predicted pulse height and angular distributions of the X-rays are in qualitative agreement with the measured values. However, the absolute magnitudes of the measured X-ray intensities, at both energies of the electrons, are smaller than the theoretical values (relativistic, nonscreened, and no backscattering considered).

INTRODUCTION

The electrons constitute an important fraction of the charged particles trapped (ref. 1) in the magnetic field of the earth. For a proper evaluation of the hazard that they present to space travel, it is necessary to consider the basic mechanism of their interaction with matter. For electrons of relatively low energy, the loss in matter is due to the excitation and ionization of bound electrons in the stopping substance. For high-energy electrons, an entirely different mechanism of energy loss, that is, the energy loss by the emission of electromagnetic radiation in the electric field of the nuclei of the stopping material, plays a prominent part. According to classical electromagnetic theory, an accelerated charge emits radiation at a rate $\frac{2}{3}\frac{e^2a^2}{c^3}$ (where a is the acceleration, e the charge, and c the velocity of the particle). An electron, on account of its small mass, can experience a large acceleration in the coulomb field of the nucleus. The resulting radiation, or bremsstrahlung as it is called, is the dominant influence in the energy loss of fast electrons. A complete discussion of energy loss of an electron by radiative collisions has been given by Bethe and Heitler (ref. 2) who used Dirac's equation for the

electron and the Born approximation for treating the interaction of electrons with the nucleus. However, use of the Born approximation is not justified for heavy elements nor for low electron energies. A number of authors (refs. 3 to 5) have tried to include other effects such as bremsstrahlung in the field of the electrons and the screening effect of atomic electrons.

From the practical standpoint, the real problem is that of thick-target radiative collisions, that is, when the electrons suffer more than one collision in passing through the target. However, few thick-target X-ray measurements (refs. 6 to 9) have been reported in the literature mainly because of the following: first, imperfect detection of the X-rays makes the analysis of observed data very difficult; second, no theoretical expressions for thick-target X-rays have been developed owing to the complex distribution of electrons, both in direction and energy, within the target. With the advent of fast electronic computers and the development of efficient phosphors for X-ray detection, both of these problems have been considerably simplified.

The subject of radiative collisions of charged particles in matter is far from being fully understood. In view of the various considerations involved in space travel, it deserves another penetrating look, both from the theoretical and the experimental standpoints. A program involving comprehensive experimental measurements on X-ray production as a function of the target material and the incident electron energies has been undertaken at the Langley Research Center. In this report, results on the X-rays produced when thick silicon targets are bombarded with 1.05 MeV and 1.25 MeV electrons are presented.

SYMBOLS

a	acceleration of charge
c	velocity of light
$\frac{-dT}{dx}$	rate of loss of energy of electrons per unit path length
E	total electron energy in units of m_0c^2
e	electron charge
$F(k)$	atomic form factor
$f(\theta)$	intensity of scattering per unit solid angle in direction θ
G_l	total average of Legendre polynomials used in describing multiple scattering, $\sum_{i=0}^{\infty} W(n)\left[<P_l \cos \theta_i > _{av}\right]^n$

I	total radiated energy in all directions; mathematically, it is obtained by integrating $I(\theta)$ over all values of θ
$I(\theta)$	total radiated energy in direction between θ and $\theta + d\theta$
$i = \sqrt{-1}$	
j, l	integers
k	photon (X-ray) energy
m_o	mass of particle at rest
N	number of target atoms per cubic centimeter
$P(\theta)d\theta$	probability that electrons are deflected between θ and $\theta + d\theta$
$P_l(\cos\theta)$	Legendre polynomial of lth order
p	electron momentum
Q	total incident charge on target
T	kinetic energy of electron
T_D	dead time of pulse height analyzer
T_o	incident electron kinetic energy
t	foil thickness, cm
v	electron velocity
$W(n)$	probability that an electron makes n collisions
$W(\theta)$	angular distribution function
Z	atomic number of target atoms
$\beta = \frac{\text{Electron velocity}}{\text{Velocity of light}} = \frac{v}{c}$	
ϵ	efficiency of X-ray production; it measures the fraction of incident energy radiated as X-rays
θ	angle between initial direction of electron and detector
λ	incident electron wavelength

$\frac{d\sigma}{dk}$	differential cross section for production of photons of energy between k and $k + dk$; mathematically, it is obtained by integrating $\frac{d\sigma^2}{dk\ d\theta}$ over all values of θ
$\frac{dn}{dk}$	total number of photons, per electron, in the energy range k, $k + dk$
$\frac{d\sigma^2}{dk\ d\theta}$	differential cross section for production of a photon lying in energy range k, $k + dk$ and emitted in direction between θ and $\theta + d\theta$
$\frac{d^2n}{dk\ d\Omega}$	total number of photons per electron per steradian in the energy range k and $k + dk$
$d\varphi(\theta)$	differential cross section for scattering in direction between θ and $\theta + d\theta$
Ω	solid angle
ψ_o	electron wave function for ground state of atom

A bar over a symbol indicates an average value.

EXPERIMENTAL DETAILS

Target Preparation

Targets have been defined as thick when their thickness equals the range of the appropriate electrons. In order to take into account the range straggling, the target thickness was made 10 percent larger than the range. The range in mg/cm^2 was calculated by using the Katz and Penfold (ref. 10) empirical formula:

$$R = 412T^n$$

where $n = 1.265 - 0.0954 \log T$ and T is the electron energy in MeV. Targets (1.5 cm × 1.0 cm) of appropriate thickness were cut from the chemically pure silicon block. The targets were cleaned ultrasonically before use.

Target Chamber

Two target chambers made of 1/8-inch-thick brass and with an inner diameter of 8 inches were used in these measurements. One of the chambers had a 14-inch-long aluminum pipe attached to the end of the chamber opposite the electron-beam entry port. This tailpipe was provided to enable the background measurement to be made without disturbing the detection setup. The other chamber had no tailpipe and was used for making X-ray measurements at angles

between 0° and 45° to the electron beam. The target chamber was mounted at the center of a 32-inch-diameter steel table of adjustable height.

Beam Integration

The target was insulated from the target chamber by means of a transparent insulating cover. The target chamber itself was insulated from the rest of the beam tube. This arrangement enabled beam alinement on the target. The charges incident on the target and the chamber (partly scattered off the target) were measured with current integrators capable of measuring currents as low as 10^{-10} ampere.

Detecting System

The X-rays were detected with a $1\frac{3}{4}$-inch by 2-inch sodium iodide crystal mounted on a photomultiplier. The detector was mounted on a rotatable steel arm at a distance of 12 inches from the target. An 8-inch-long lead collimator with a tapered axial clearance leading to the center of the target was placed between the chamber and the detector. The collimator hole was 0.925 inch in diameter at the face in contact with the crystal. The hole diameter had a gradient of 0.074 inch per inch. In order to take into account variation in beam intensity, the interaction was monitored with another $1\frac{3}{4}$-inch by 2-inch sodium iodide crystal also mounted on a photomultiplier and located at a distance of 11 inches from the target at an angle of 52° on the opposite side of the beam line. A 6-inch-long collimator similar to the one used with the main detector was used with the monitor crystal. The monitor counter output, after suitable amplification and pulse shaping, was fed into a single-channel pulse-height analyzer biased to reject all pulses less than 500 keV in energy. The output of the analyzer was then fed to a fast scaler.

The output of the movable counter, after suitable amplification, was fed into a 400-channel pulse height analyzer. The data were then fed into a paper tape punch and later transcribed using a paper tape reader and a typewriter.

Experimental Procedure

Electron beams of the order of a few nanoamperes and energy 1.05 MeV and 1.25 MeV from the 1.25 MeV electron accelerator were focused on the target with the help of a magnetic lens located close to the base of the beam tube. The beam size was further reduced with the help of carbon collimators located between the target chamber and the lens.

The electron beam was centered on the target with the aid of a television camera. The X-ray spectra were measured with the target in the path of the beam and with the target pulled up so as to allow the beam to hit the end of the long aluminum pipe. The counting rate in the main detector when the beam

hit the pipe was less than 2 percent of the counting rate when the target was bombarded. The corrections for the background counts were made in the following manner.

Suppose the charge collected by the chamber when the beam is incident on the target is Q_1. The average distance of the points where the scattered electrons strike the target chamber is equal to the distance of the beam line from the detector. For the purpose of measuring distance between the effective site of background counts and the detector, the effective site has been taken as a point 2 inches ahead of the target on the beam line. Suppose this distance is d_1. Suppose the charge incident on the aluminum pipe when the target is pulled out of the beam is Q_2. Let the distance between the detector and the point where the electrons strike the aluminum extension pipe be d_2. If the counting rate from this latter configuration be c_2, the actual background counting rate c_1 is given by the following relation:

$$c_1 = c_2\left(\frac{d_2}{d_1}\right)^2\left(\frac{Q_1}{Q_2}\right)\left(\frac{Z_{Brass}}{Z_{Al}}\right)^2 \qquad (1)$$

In this relation, two tacit assumptions have been made:

(1) Equal shielding of the main detector from all sides

(2) The contribution due to the scattered electrons is of the same order as that due to the incident electrons.

The second assumption is not strictly justifiable in view of the reduced electron energy; but overall low background counting rate makes this assumption essentially redundant.

The pulse-height distribution measurements were repeated at seven angles between 45° and 130° for a fixed number of monitor counts. In order to measure the spectra along directions inclined at angles of less than 45° to the electron beam, the second chamber, without the aluminum tailpipe, was used. In order to compare the spectra taken with the two different target chambers, overlapping measurements were made at three different angles. From these three common spectra, an average normalizing factor was obtained. The measurements at angles below 45° were corrected by this factor.

Figures 1 and 2 show the target chamber and the block diagram of the experimental setup, respectively. Figure 3 shows a typical X-ray spectrum and the background spectrum.

ANALYSIS OF THE DATA

Before the experimental results can be compared with any theory, the data have to be corrected for the effects of the detecting system. In the present case, corrections have been made for the following effects: counting rate, finite resolution, and detection efficiency.

Counting-Rate Effect

The pulse height analyzer does not register all the pulses arriving at the gate because of a finite dead time. (The dead time in microseconds of the analyzer used is given by the expression:

$$T_D = 39 + 0.4N'$$

where N' is the channel number where counts are stored.) This dead time is a function of the height of the incoming pulses. The fraction of the time wasted because of the dead time associated with each incoming pulse depends on the counting rate which varies from angle to angle. One way of allowing for this effect is to measure simultaneously the clock time duration of the measurement and live time. The analyzer keeps its own record of the live time. The ratio of these two times gives a factor by which all the observed counts at a particular angle must be corrected. Since the background counting rate is much less than the main counting rate, respective counting-rate corrections must be made before the background counts are subtracted from the main counts.

Finite Resolution Effect

A monoenergetic photon beam does not produce a pulse of unique height from a sodium iodide phosphor. This condition is due to the fact that the incident photons may deposit energy between zero and the maximum possible within the phosphor, depending on their paths within it. Thus, a monoenergetic X-ray source produces pulses varying in height from approximately zero to the maximum possible. This variation makes the analysis of a continuous-energy X-ray spectrum very difficult.

In order to correct the experimental spectrum for this effect, reference spectra should be taken from a number of suitable monoenergetic gamma sources. The observed spectrum should then be unfolded by drawing in appropriate individual spectra. In the present investigation, Na^{22} (0.51, 1.28 MeV), Cs^{137} (0.667 MeV), and Co^{60} (1.17, 1.33 MeV) gamma sources were used to provide the reference spectral shapes. (See fig. 4 for Cs^{137} and Co^{60}.) The following analytical procedure was adopted: Starting from the high-energy end, the observed spectrum was divided into 50 keV wide intervals. A component spectrum with the intensity of the total capture peak equal to the mean interval intensity and the peak energy equal to the mean interval energy was drawn in the highest energy interval. Allowance for the fact that the X-ray energy spread

within an interval is 50 keV was made by appropriately broadening the monoenergetic reference shape. This component spectrum was subtracted from the observed spectrum and the next pulse profile (with energy 50 keV less) was then drawn in and subtracted in the same manner. This process was continued until the lower energy end of the observed spectrum was reached. The area under each component spectrum was then measured. This area corresponded to the intensity of the pulses with energy equal to the corresponding mean interval energy. Figure 5 illustrates the unfolding procedure.

Detection Efficiency Effect

The detection efficiency of the sodium iodide crystal is a function of the incident X-ray energy. The detection efficiency of the crystal has been calculated theoretically by assuming that each photon travels a distance of 2 inches through the crystal. Figure 6 shows the efficiency as a function of energy. To correct for the effects of detection efficiency for X-rays of different energies, the observed intensities after the counting-rate correction was made were divided by the appropriate efficiency factor.

This procedure was followed for correcting the observed spectrum at each angle. The data thus obtained have been consolidated as follows:

(a) Each spectrum has been broken up into three groups: high-energy group, intermediate-energy group, and low-energy group

The angular distribution of the X-rays in each group has been expressed as follows:

$$W(\theta) = \sum_{l=0}^{4} a_l P_l(\cos\theta) \tag{2}$$

where $P_l(\cos\theta)$ is the Legendre polynomial of the lth order. Figures 7(a) and 7(b) show the angular distribution of the three groups, and the numerical results are given in table I. The angular distribution of high-energy photons is seen to be more sharply peaked in the forward direction than that of low-energy photons.

(b) At each angle, the total radiated energy has been calculated in the following manner:

$$I(\theta) = \sum_{k=0}^{T_o} k\,N(k) \tag{3}$$

where

k X-ray energy

$N(k)$ number of X-rays with energy equal to k

T_o kinetic energy of incident electrons; also equals the maximum photon energy

Since the nucleus is heavy compared with the electron, the momentum of the electron plus light quantum is not, in general, conserved; the nucleus can take any amount of momentum. A finite transition probability to any final state E,p which satisfies $T + k = T_o$ is obtained. (See refs. 11 to 13.)

The observed values of total radiated energy at each angle have been fitted to an expression of the form given by equation (2). Figures 8(a) and 8(b) show the angular distribution of radiated energy at two electron energies. The numerical results are given in table II.

(c) The observed intensity of the X-rays in each strip at each angle has been integrated over all directions in space. In this way, $\frac{d\sigma^2}{dk\ d\theta}$ has been obtained at each electron energy and $\frac{d\sigma}{dk}$ has then been obtained by evaluating $\int_0^\pi \frac{d^2\sigma}{dk\ d\theta} \sin\theta\ d\theta$ at each electron energy. The results are shown in figures 9 and 10.

(d) The total radiated energy at each angle $I(\theta)$ has been integrated over all directions in space to give the entire radiated energy I. This procedure enabled a calculation of the efficiency of X-ray production as follows:

$$\epsilon = \frac{\text{Total radiated energy}}{\text{Total incident electron energy}} = \frac{I}{nT_o} \qquad (4)$$

where n is the number of incident electrons and is equal to $\frac{\text{Total incident charge}}{\text{Charge per electron}}$. The results are given in table III.

THEORY

All bremsstrahlung theories predict the probability of emission of electromagnetic radiation in a single encounter between the incident electron and the target nucleus. In this encounter, there is no ambiguity about the direction and energy of the incident electron. But when an electron is passing through a thick foil, its direction as well as energy are continuously changing. It is therefore necessary to keep track of the directions and energies of the electrons at all stages of their progress through the stopping medium for a proper evaluation of the thick target bremsstrahlung spectrum. This is an extremely tedious and time-consuming process. Before outlining a practical approach to the solution of this problem, a brief discussion of various factors that affect electron paths and energies is given.

Elastic Scattering of Electrons by Atoms

More probable than the electron-electron collisions are the collisions between the incident electrons and the atoms of the stopping material. In these latter collisions, the electrons are merely deflected with no loss of energy. Accurate treatments of nonrelativistic single scattering using the Fermi-Thomas atomic model and the Born approximation have been given by Bethe (ref. 14) and by Bullard and Massey (ref. 15). The differential cross section for scattering through an angle θ into the solid angle $2\pi \sin\theta \, d\theta$ is given by

$$d\phi(\theta) = \frac{2\pi e^4}{4p^2v^2}(Z - F(k))^2 \frac{\sin\theta \, d\theta}{\sin^4 \frac{\theta}{2}} \tag{5}$$

where $F(k)$ is the atomic form factor given by

$$F(k) = \int \sum_{j=1}^{Z} e^{ik\cdot r_j} \left|\psi_o\right|^2 d\tau \tag{6}$$

and

ψ_o electronic wave function for ground state of atom

$i = \sqrt{-1}$

r_j position vector for jth electron

$d\tau$ volume element

Moliére (ref. 16) has derived a similar expression for a screened coulomb field without the use of the Born approximation. For relativistic velocities, the shielding effects are confined to smaller angles. Mott (refs. 17 and 5) calculated differential scattering cross section from an unscreened coulomb field for relativistic electrons by using the following expression:

$$d\phi(\theta) = \frac{2\pi e^4 Z^2}{4p^2v^2} \frac{\sin\theta \, d\theta}{\sin^4 \frac{\theta}{2}} \left[1 - \beta^2 \sin^2 \frac{\theta}{2} - \frac{Z\pi\beta}{137} \sin \frac{\theta}{2}\left(\sin^2 \frac{\theta}{2} - 1\right)\right] \tag{7}$$

However, use of the Born approximation - made in this derivation - is not justified even at high energies except for very light nuclei. The number of electron-atom elastic collisions is very large and they produce characteristic multiple scattering effects even for thin foils. Multiple scattering has been considered by a number of authors. For foils and incident energies when multiple scattering takes place but energy losses can be neglected, Williams

(refs. 18 and 5) has shown that the statistical distribution of angular deflections is given by the Gaussian distribution:

$$P(\theta)d\theta = \frac{2}{\overline{\theta^2}}\,\theta\left(e^{-\theta^2/\overline{\theta^2}}\right)d\theta \tag{8}$$

where

$$\overline{\theta^2} = t\,\frac{4\pi NZ(Z+1)e^4(1-\beta^2)}{m_o^2v^4}\,\log\left[4\pi Z^{1/3}(Z+1)Nt\left(\frac{h/2\pi}{mv}\right)^2\right] \tag{9}$$

h is Planck's constant, and t is the foil thickness in centimeters. This simplified theory is not complete because it does not hold for very large angles and does not include the scatterings in which more than one deflection takes place although not enough are involved to give the characteristic Gaussian distribution. The basic theory of multiple scattering has been given by Goudsmit and Saunderson (refs. 19 and 20) and more recently by Moliére (ref. 21). The results of these theories are given below.

The normalized probability $f(\theta)d\Omega$ that the electron will be deflected into an angle between θ and $\theta + d\theta$, after it has traveled a path length t through the scattering material of atomic number Z, containing N atoms per cubic centimeter, is given by the following series in Legendre polynomials:

$$f(\theta)d\Omega = \frac{1}{2}\sum_{l}(2l+1)G_lP_l(\cos\theta)\sin\theta\,d\theta \tag{10}$$

The coefficients G_l are given by

$$G_l = \exp\left\{-2\pi N\int_{T_o}^{T_i}\int_0^{\pi}\sigma(T,\theta')\left[1 - P_l(\cos\theta')\right]dT\,d\theta'\right\} \tag{11}$$

where

T_o kinetic energy of incident electron

T_i kinetic energy of electron in ith strip

N number of target atoms per cubic centimeter

and the corrected Rutherford scattering cross section $\sigma(T,\theta')$ is given by

$$\sigma(T,\theta') = \frac{Z^2e^4}{p^2v^2(1 - \cos\theta' + 2\eta)^2} \tag{12}$$

where the screening parameter for electrons is given by Moliére as

$$\eta = \left(1.7 \times 10^{-5}\right)Z^{2/3}\left[1.13 + 3.76\left(\frac{Z}{137\beta}\right)^2\right] \tag{13}$$

Electron-Electron Scattering

The theory of the energy loss of an electron by inelastic encounters with the electrons in the stopping material has been worked out by Bethe. (See ref. 22.) For nonrelativistic electrons, the result is

$$-\frac{dT}{dx} = \frac{4\pi e^4 N}{mv^2} Z \log_e \frac{mv^2}{2I}\sqrt{e/2} \tag{14}$$

where

N number of target atoms per cubic centimeter

I average excitation potential of atom

Z target nucleus charge

Bethe, by using Moller's formula (ref. 23) for the scattering of electrons by electrons, has also calculated the stopping power of various materials for relativistic electrons. The result is

$$-\frac{dT}{dx} = \frac{2\pi Ne^4}{mv^2} Z\left[\log \frac{m_o v^2 T_o}{2I^2\left(1 - \beta^2\right)} - \left(2\sqrt{1 - \beta^2} - 1 + \beta^2\right)\log 2 + \left(1 - \beta^2\right) + \frac{1}{8}\left(1 - \sqrt{1 - \beta^2}\right)^2\right] \tag{15}$$

where

T_o kinetic energy of incident electron

$\beta = \frac{v}{c}$

In this way, one expects a continuous energy loss by the electrons as they penetrate thick foils. The rate of loss of energy is continuously increasing as the velocity of the electrons decreases (that is, as the electrons penetrate farther). Besides the effects associated with the distribution in space and energy for the electrons, another effect, namely, the attenuation effect of the rest of the target foil on the bremsstrahlung, must also be considered.

As indicated earlier, these effects are very difficult to handle in exactness. However, it is possible to introduce certain simplifications without reducing the rigor of the treatment appreciably. In the first place, electron-atom and electron-electron scattering can be regarded as essentially independent of each other. This procedure enables one to treat the thick foil as made up of a large number of thin foils, each producing the same energy loss through excitation and/or ionization. Multiple scattering effects in each foil can be evaluated. The absorption effects of the target can be approximately allowed for by assuming that, on the average, each photon will have to travel through half the thickness of the target. The absorption effects are important mainly for the low-energy photons and they are likely to be produced all along the electron tracks with a slightly diminishing probability.

With these simplifications, the thick target case can be reduced to the following schematic form (sketch (a)):

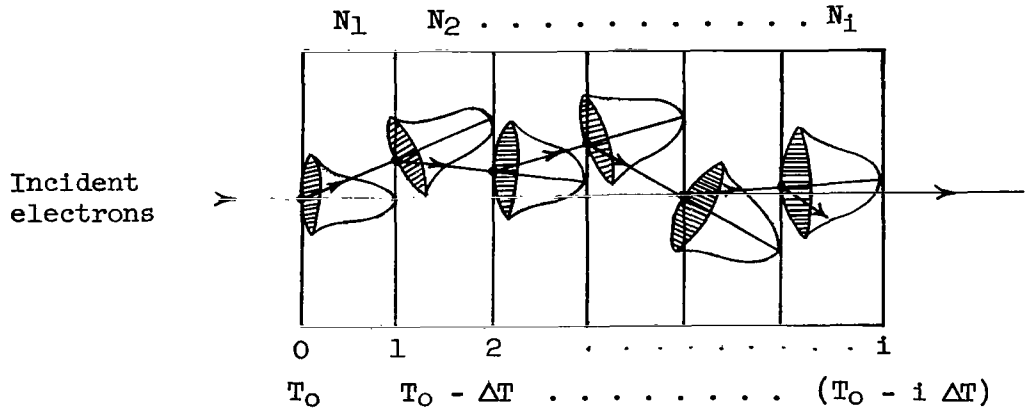

Sketch (a)

where

N number of target atoms per cubic centimeter

$\Delta E = 50$ keV

N_i number of target atoms in the ith strip and proportional to statistical weight of ith strip

The probability of scattering of an electron in any given direction is given by the differential cross section for multiple scattering in that direction. Due regard must be given to the fact that the electron distribution is symmetric in space about the direction of propagation of electrons in the beginning of each strip. Thus an electron, although scattered through the same average angle θ, may be traveling in an entirely different direction with respect to the detector. This effect can be allowed for as indicated in sketch (b):

where

$$BD = x \tan \beta_j$$

$$AD = x \sec \beta_j$$

$$BC = x \tan \theta$$

$$AC = x \sec \theta$$

and

$$\cos \gamma_{jl} = \cos \theta \cos \beta_j (1 + \tan \theta \tan \beta_j \cos \phi_l)$$

$$= \cos \theta \cos \beta_j + \sin \theta \sin \beta_j \cos \phi_l \qquad (16)$$

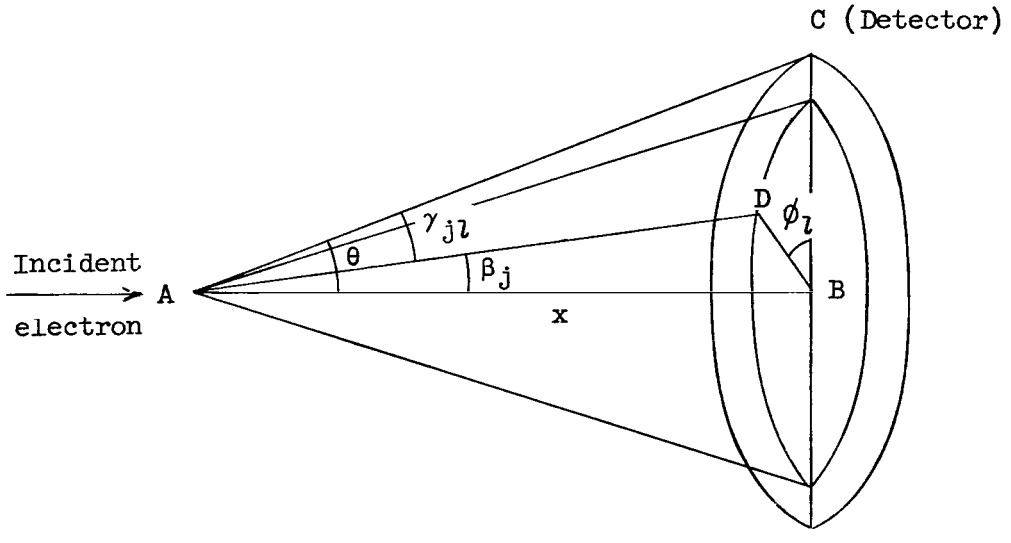

Sketch (b)

It has been assumed that the lateral displacement of the electrons due to multiple scattering is extremely small compared with the distance of the detector from the target. Thus, multiple scattering effectively changes only the direction of incidence of the electron involved in radiative collision. This assumption is not unreasonable (refs. 24 and 25) in the case considered.

If one follows the progress of a large number of electrons through all the strips and keeps track of their directions in successive strips, one can get the over-all $\frac{d^2\sigma}{dk\ d\theta}$ and $\frac{d\sigma}{dk}$. (See appendix.) The cross-section differential in pulse height $\frac{d\sigma}{dk}$ is calculated from $\frac{d^2\sigma}{dk\ d\theta}$ by integrating it over all directions in space.

$$\frac{d^2\sigma}{dk\ d\theta} = \sum_l \sum_j \sum_i N_i \left[\frac{d^2\sigma}{d\beta\ d\phi}\left(T_i, \beta_j, \phi_l\right)\right]_{\text{multiple scattering}} \left[\frac{d^2\sigma}{dk\ d\gamma}\left(T_i, k, \gamma_{jl}\right)\right]_{\text{Bethe-Heitler}} \left[e^{-\frac{\mu(k)x}{2\cos\theta}}\right] \qquad (17)$$

where

N_i number of atoms in ith strip

T_i electron energy in ith strip

β_j semiangle of cone (see sketch (b))

ϕ_l azimuthal angle

γ_{jl} angle between incident electron and emitted proton

k energy of photon

$\mu(k)$ attenuation coefficient in silicon for photons of energy k, cm^{-1}

θ angle between incident electron beam and detector

$\frac{d^2\sigma}{d\beta\ d\phi}$ multiple scattering cross section calculated from Goudsmit-Saunderson theory

$\frac{d^2\sigma}{dk\ d\gamma}$ radiative collision cross section as given by Bethe-Heitler theory

x range of incident electrons in target

Target thickness is measured in centimeters.

COMPARISON BETWEEN THEORY AND EXPERIMENT

At electron energies of the order of one million volts and above, exact electron Dirac wave functions must be used to calculate theoretical bremmstrahlung cross sections. However, to date, no such calculations have been

successful. Consequently, the only predictions of $\frac{d^2\sigma}{dk\ d\theta}$ and $\frac{d\sigma}{dk}$ that are directly comparable with the present experiment are those of Bethe-Heitler and others obtained by means of Born approximation. For comparison at low energies, Heitler (ref. 11) has given estimates of the error resulting from the use of Born approximation in the nonrelativistic energy range.

Comparison between the theory (relativistic) and the experiment is shown in figures 9 and 10. The effects of screening of the nuclear field by the atomic electrons and the backscattering of electrons from the target have not been included in these theoretical calculations because of the lack of reliable information on these effects. The energy loss straggling in collision with atomic electrons has also been ignored. The errors on the experimental points range from about 10 percent in the low-energy region to about 20 percent in the intermediate energy region. The errors on the points close to the high energy end of the spectrum are of the order of 50 percent. Figure 9 shows that the absolute magnitude of the X-ray intensities integrated over all directions is not in good agreement with the predictions of the Bethe-Heitler theory. However, the inclusion of the backscattering effects and statistical fluctuations in the ionization loss are expected to bring the two curves in reasonably good agreement. Figure 10 shows comparison between experimental and theoretical pulse height distribution spectra at $\theta = 45^{\circ}$. It is seen that the experimental curve crosses the theoretical curve at about the middle of the spectrum, the experimental curve being lower in the low-energy region and higher in the high-energy region.

The total radiated intensity per electron, integrated over all directions in space, has been measured. From these measurements, the efficiency of X-ray production has been calculated to be 0.65 percent at an electron energy of 1.05 MeV and 0.75 percent at an electron energy of 1.25 MeV (see table III) compared with the corresponding theoretical values of 0.71 percent and 0.89 percent.

It thus appears that the Bethe-Heitler theory, suitably corrected for screening effects of atomic electrons and proper account of electron multiple scattering being taken, may give a reasonable account of radiative collision cross sections of electrons with silicon atoms. The use of Sommerfeld theory (ref. 26) for nonrelativistic energy region may improve the agreement.

CONCLUDING REMARKS

Measurements have been made on the X-rays produced when thick silicon targets are bombarded with 1.05 MeV and 1.25 MeV electrons. The various cross sections have been compared with those predicted by the Bethe-Heitler theory. This comparison indicates that the Bethe-Heitler theory, when suitably corrected

for screening effects of atomic electrons and multiple scattering of the incident electrons, may give a reasonable account of radiative collision cross sections of electrons with silicon atoms. The use of the Sommerfeld theory for nonrelativistic energy region may improve the agreement.

Langley Research Center,
National Aeronautics and Space Administration,
Langley Station, Hampton, Va., August 14, 1964.

APPENDIX

RADIATIVE COLLISION CROSS SECTIONS OF ELECTRONS IN MATTER

As indicated in reference 4 a large number of investigators have attempted to evaluate bremsstrahlung production when swift electrons strike matter. For comparing the data with theory, formulas 2BN and 3BN of reference 4 will be used.

$$\frac{d^2\sigma}{dk\,d\theta} = \frac{Z^2 r_o^2}{4(137)} \frac{p \sin\theta_o}{k p_o} \left\{ \frac{8 \sin^2\theta_o (2E_o^2 + 1)}{p_o^2 \Delta_o^4} - \frac{2(5E_o^2 + 2EE_o + 3)}{p_o^2 \Delta_o^2} - \frac{2(p_o^2 - k^2)}{Q^2 \Delta_o^2} \right.$$

$$+ \frac{4E}{p_o^2 \Delta_o} + \frac{L}{p p_o} \left[\frac{4E_o \sin^2\theta_o (3k - p_o^2 E)}{p_o^2 \Delta_o^4} + \frac{4E_o^2 (E_o^2 + E^2)}{p_o^2 \Delta_o^2} \right.$$

$$\left. + \frac{2 - 2(7E_o^2 - 3EE_o + E^2)}{p_o^2 \Delta_o^2} + \frac{2k(E_o^2 + EE_o - 1)}{p_o^2 \Delta_o} \right]$$

$$\left. - \left(\frac{4\epsilon}{p\,\Delta_o}\right) + \left(\frac{\epsilon^Q}{pQ}\right) \left[\frac{4}{\Delta_o^2} - \frac{6k}{\Delta_o} - \frac{2k(p_o^2 - k^2)}{Q^2 \Delta_o} \right] \right\} \qquad (18)$$

where

$$L = \log_e \left[\frac{EE_o - 1 + pp_o}{EE_o - 1 - pp_o} \right]$$

$$\Delta_o = E_o - p_o \cos\theta_o$$

$$\epsilon = \log_e \left(\frac{E + p}{E - p} \right)$$

$$\epsilon^Q = \log_e \left(\frac{Q + p}{Q - p} \right)$$

$$Q^2 = p_o^2 + k^2 - 2p_o k \cos\theta_o$$

$$\frac{d\sigma}{dk} = \frac{Z^2 r_o^2}{137}\frac{p}{kp_o}\left\{\frac{4}{3} - 2E_oE\frac{p^2 + p_o^2}{p^2p_o^2} + \frac{\epsilon_oE}{p_o^3} + \frac{\epsilon E_o}{p^3} - \frac{\epsilon\epsilon_o}{pp_o}\right.$$

$$+ L_1\left[\frac{8E_oE}{3p_op} + \frac{k^2\left(E_o^2E^2 + p_o^2p^2\right)}{p_o^3p^3} + \frac{k}{2p_op}\left(\frac{E_oE + p_o^2}{p_o^3}\epsilon_o\right.\right.$$

$$\left.\left.\left. - \frac{E_oE + p^2}{p^3}\epsilon + \frac{2kE_oE}{p^2p_o^2}\right)\right]\right\} \qquad (19)$$

where

$$L_1 = 2\log_e\frac{E_oE + p_op - 1}{k}$$

$$\epsilon_o = \log_e\frac{E_o + p_o}{E_o - p_o}$$

In these two expressions, the units are slightly different from those of the text. All the quantities used are defined as follows:

E_o, E initial and final total energy of the electron, mc^2

p_o, p initial and final momentum of the electron, mc

k energy of photons, mc^2

θ_o angle between p_o and k

r_o classical electron radius, $\frac{e^2}{mc^2} = 2.82 \times 10^{-13}$ cm

$\beta = \frac{p}{E} = \frac{\text{Final momentum}}{\text{Final energy}}$ of electron

$\beta_o = \frac{p_o}{E_o} = \frac{\text{Initial momentum}}{\text{Initial energy}}$ of electron

REFERENCES

1. Van Allen, James A.: Radiation Belts Around the Earth. Sci. Am., vol. 200, no. 3, Mar. 1959, pp. 39-47.

2. Bethe, H.; and Heitler, W.: Stopping of Fast Particles and Creation of Electron Pairs. Proc. Roy. Soc. (London), vol. 146, Aug. 1, 1934, pp. 83-112.

3. Bethe, Hans A.; and Ashkin, Julius: Passage of Radiations Through Matter. Experimental Nuclear Physics, Vol. I, E. Segrè, ed., John Wiley & Sons, Inc., c.1953, pp. 166-357.

4. Koch, H. W.; and Motz, J. W.: Bremsstrahlung Cross-Section Formulas and Related Data. Rev. Mod. Phys., vol. 31, no. 4, Oct. 1959, pp. 920-955.

5. Birkhoff, R. D.: The Passage of Fast Electrons Through Matter. Encyclopedia Phys., vol. XXXIV, Corpuscles and Radiation in Matter II, S. Flügge, ed., Springer-Verlag (Berlin), 1958, pp. 53-138.

6. Buechner, W. W.; Van de Graaff, R. J.; Burrill, E. A.; and Sperduto, A.: Thick-Target X-Ray Production in the Range From 1250 to 2350 Kilovolts. Phys. Rev., Second ser., vol. 74, no. 10, Nov. 15, 1948, pp. 1348-1352.

7. Miller, William; Motz, J. W.; and Cialella, Carmen: Thick Target Bremsstrahlung Spectra for 1.00-, 1.25-, and 1.40-Mev Electrons. Phys. Rev., Second ser., vol. 96, no. 5, Dec. 1, 1954, pp. 1344-1350.

8. Motz, J. W.: Bremsstrahlung Differential Cross-Section Measurements for 0.5- and 1.0-Mev Electrons. Phys. Rev., Second ser., vol. 100, no. 6, Dec. 15, 1955, pp. 1560-1571.

9. Wilson, Richard: A Formula for Thick Target Bremsstrahlung. Proc. Phys. Soc. (London), vol. 66, pt. 7, no. 403A, July 1, 1953, pp. 638-644.

10. Katz, L.; and Penfold, A. S.: Range-Energy Relations for Electrons and the Determination of Beta-Ray End-Point Energies by Absorption. Rev. Mod. Phys., vol. 24, no. 1, Jan. 1952, pp. 28-44.

11. Heitler, W.: The Quantum Theory of Radiation. Third ed. The Clarendon Press (Oxford), 1954.

12. Fano, U.; Koch, H. W.; and Motz, J. W.: Evaluation of Bremsstrahlung Cross Sections at the High-Frequency Limit. Phys. Rev., Second ser., vol. 112, no. 5, Dec. 1, 1958, pp. 1679-1683.

13. Fermi, E. (Jay Orear, A. H. Rosenfeld, and R. A. Schluter, compilers): Nuclear Physics. Rev. ed., Univ. of Chicago Press, 1950.

14. Bethe, H.: Zur Theorie des Durchgangs schneller Korpus-kularstrahlen durch Materie. Ann. Physik, vol. 5, no. 3, June 10, 1930, pp. 325-400.

15. Bullard, E. C.; and Massey, H. S. W.: Scattering of Electrons by Atomic Fields. Proc. Cambridge Phil. Soc., vol. 26, Oct. 1930, pp. 556-563.

16. Molière, G.: Theory of Scattering of Fast Charged Particles. II. Plural and Multiple Scattering. Naturforsch., vol. 3a, Feb. 1948, pp. 78-97.

17. Mott, N. F.: The Polarisation of Electrons by Double Scattering. Proc. Roy. Soc. (London), vol. 135, Mar. 1, 1932, pp. 429-458.

18. Williams, E. J.: Multiple Scattering of Fast Electrons and Alpha-Particles, and "Curvature" of Cloud Tracks Due to Scattering. Phys. Rev., Second ser., vol. 58, no. 4, Aug. 15, 1940, pp. 292-306.

19. Goudsmit, S.; and Saunderson, J. L.: Multiple Scattering of Electrons. Phys. Rev., Second ser., vol. 57, no. 1, Jan. 1, 1940, pp. 24-29.

20. Goudsmit, S.; and Saunderson, J. L.: Multiple Scattering of Electrons. II. Phys. Rev., Second ser., vol. 58, no. 1, July 1, 1940, pp. 36-42.

21. Molière, Gert: Theory of Scattering of Fast Charged Particles. Part I.- Single Scattering by the Shielded Coulomb Field. Transl. 19G5G, Assoc. Tech. Services (East Orange, N.J.), Mar. 1955.

22. Bethe, H.: Quantenmechanik der Ein- und Zwei-Elektronenprobleme. Handb. Phys., Bd. XXIV, Kap. 3, Julius Springer (Berlin), 1933, pp. 273-560.

23. Moller, C.: Passage of Hard β-Rays Through Matter. Ann. Physik, vol. 14, no. 5, Aug. 15, 1932, pp. 531-585.

24. Rossi, Bruno; and Greisen, Kenneth: Cosmic-Ray Theory. Rev. Mod. Phys., vol. 13, no. 4, Oct. 1941, pp. 240-309.

25. Blatt, John M.: Theoretical Analysis of Ionization Chamber Data on Large Air Showers. Phys. Rev., Second ser., vol. 75, no. 10, May 15, 1949, pp. 1584-1598.

26. Sommerfeld, A.: On the Diffraction and Stopping of Electrons. Ann. Physik, vol. 11, 1931, pp. 257-330.

TABLE I.- ANGULAR DISTRIBUTION OF THE X-RAYS PRODUCED WHEN 1.05 MeV AND 1.25 MeV ELECTRONS BOMBARDED THICK SILICON TARGETS

Electron energy, MeV	Energy interval, keV	Angular distribution expression, W(θ) (*)
1.05	750 to 1050	$P_0 + 1.85P_1 + 1.51P_2 + 0.88P_3 + 0.40P_4$
	450 to 750	$P_0 + 1.38P_1 + 0.86P_2 + 0.50P_3 + 0.20P_4$
	150 to 450	$P_0 + 0.73P_1 + 0.12P_2 + 0.29P_3 + 0.06P_4$
1.25	850 to 1250	$P_0 + 1.70P_1 + 2.11P_2 + 0.90P_3 + 0.87P_4$
	450 to 850	$P_0 + 1.48P_1 + 0.97P_2 + 0.49P_3 + 0.30P_4$
	100 to 450	$P_0 + 0.69P_1 + 0.27P_2 + 0.17P_3 + 0.22P_4$

*$P_l = P_l(\cos\theta)$ where $l = 0, 1, 2, 3$.

TABLE II.- ANGULAR DISTRIBUTION OF TOTAL RADIATED ENERGY FROM THICK SILICON TARGETS BOMBARDED WITH 1.05 MeV AND 1.25 MeV ELECTRONS

Electron energy, MeV	Angular distribution expression, W(θ) (*)
1.05	$P_0 + 0.88P_1 + 0.35P_2 + 0.32P_3 + 0.15P_4$
1.25	$P_0 + 0.93P_1 + 0.54P_2 + 0.36P_3 + 0.31P_4$

*$P_l = P_l(\cos\theta)$ where $l = 0, 1, 2, 3$.

TABLE III.- EFFICIENCY OF RADIATIVE COLLISIONS IN SILICON

Electron energy, MeV	Results of present investigation, percent (*)		Theoretical results, percent (**)
	$\frac{\sum_{100\text{ keV}}^{T_0} \text{Radiated energy}}{\text{Incident energy}}$	$\frac{\text{Total radiated energy}}{\text{Incident energy}}$	
1.05	0.32	0.65	0.71
1.25	0.37	0.75	0.89

*In the calculations, the absorption of X-rays in target and air has not been considered. Also, the curves were extrapolated to get radiated flux in the direction of incident electrons.

**Refs. 2, 5, and 12.

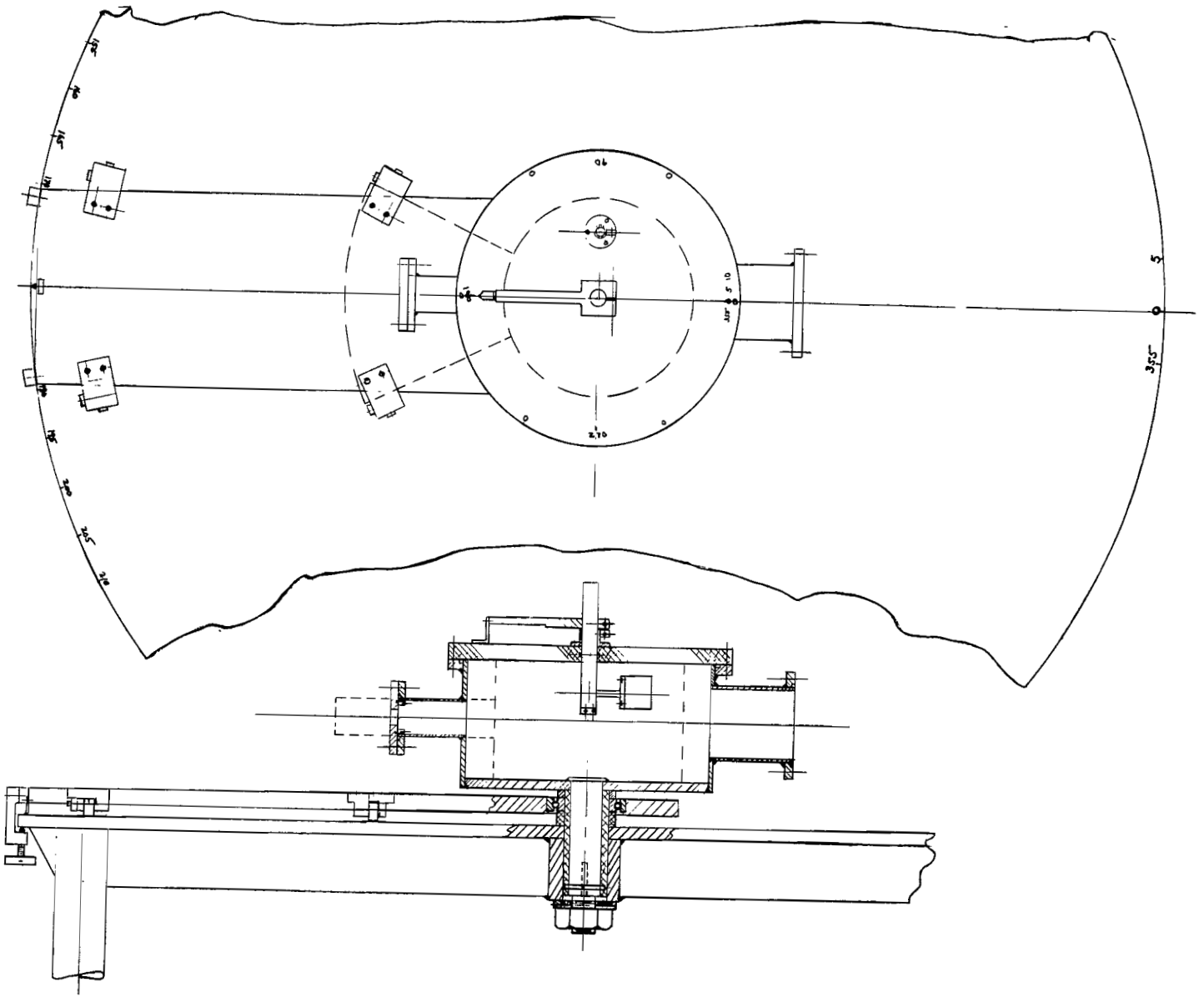

Figure 1.- View of target chamber.

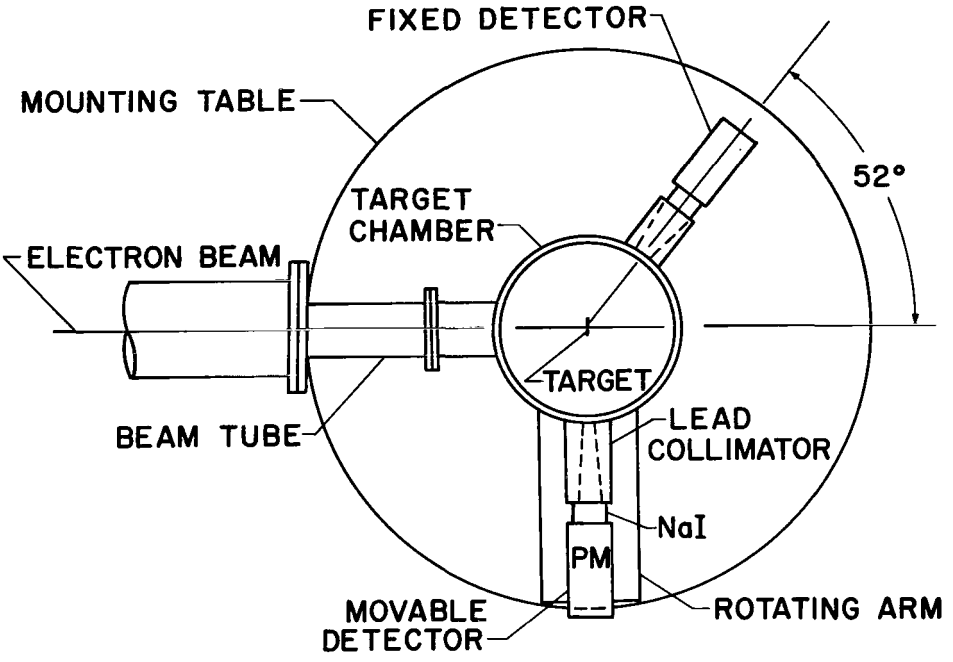

Figure 2.- Block diagram of detection system.

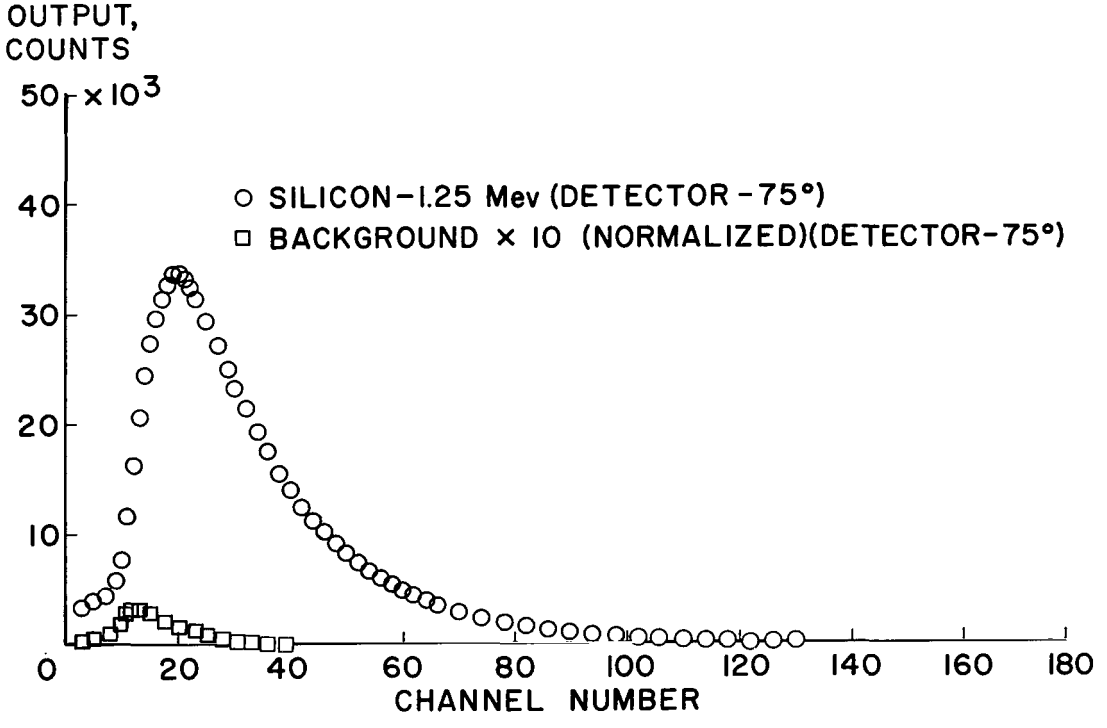

Figure 3.- Comparison of target bremsstrahlung spectrum with background spectrum.

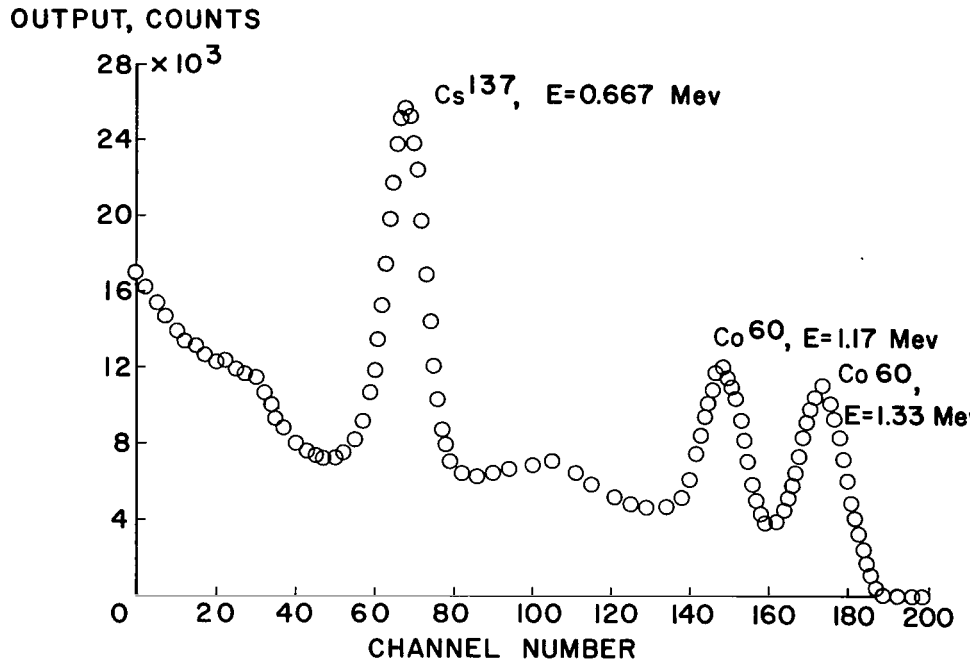

Figure 4.- Reference spectral shapes (Cs^{137} and Co^{60}).

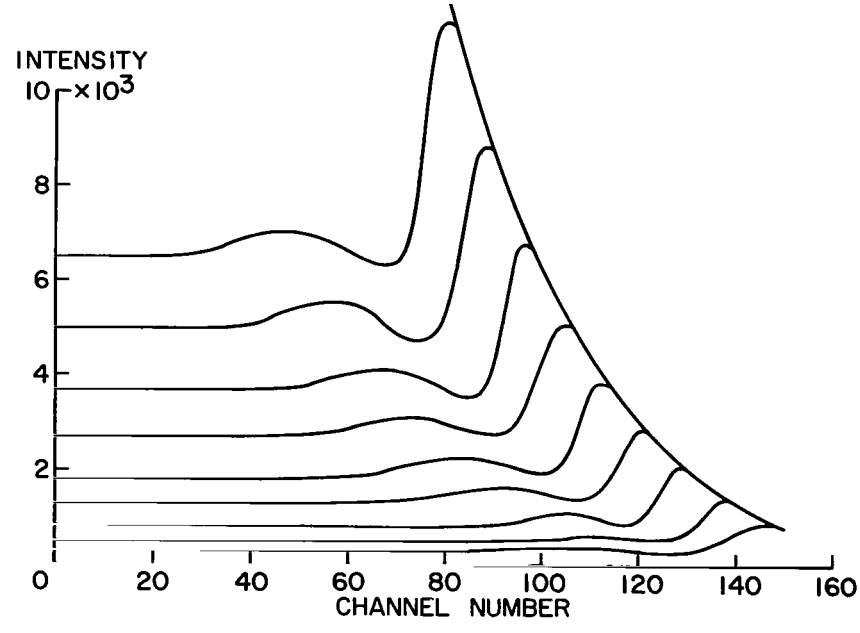

Figure 5.- An illustration of spectrum stripping.

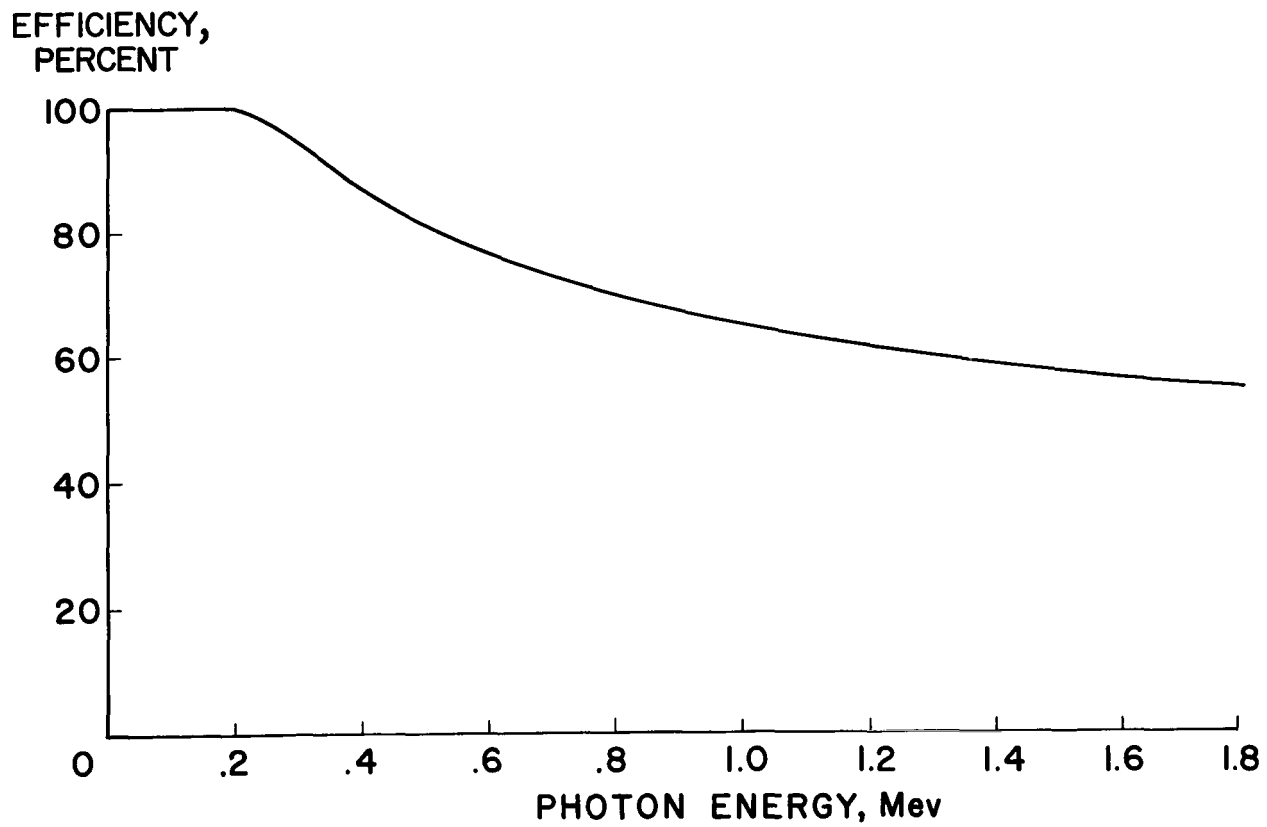

Figure 6.- Variation of efficiency of sodium iodide crystal with the X-ray energy.

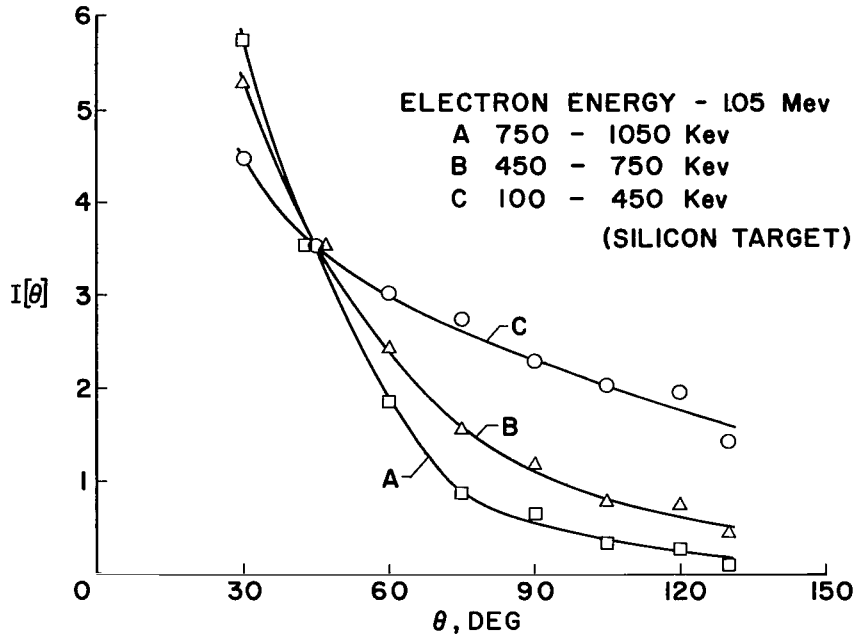

(a) Silicon at 1.05 MeV.

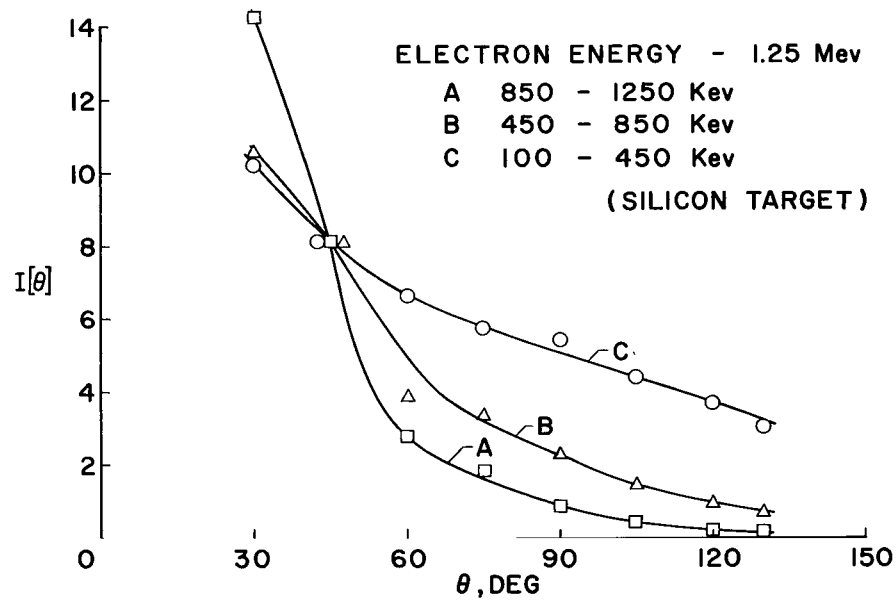

(b) Silicon at 1.25 MeV.

Figure 7.- Angular distribution of three sections of X-ray spectrum. The intensities have been adjusted to be the same at 45° for each group.

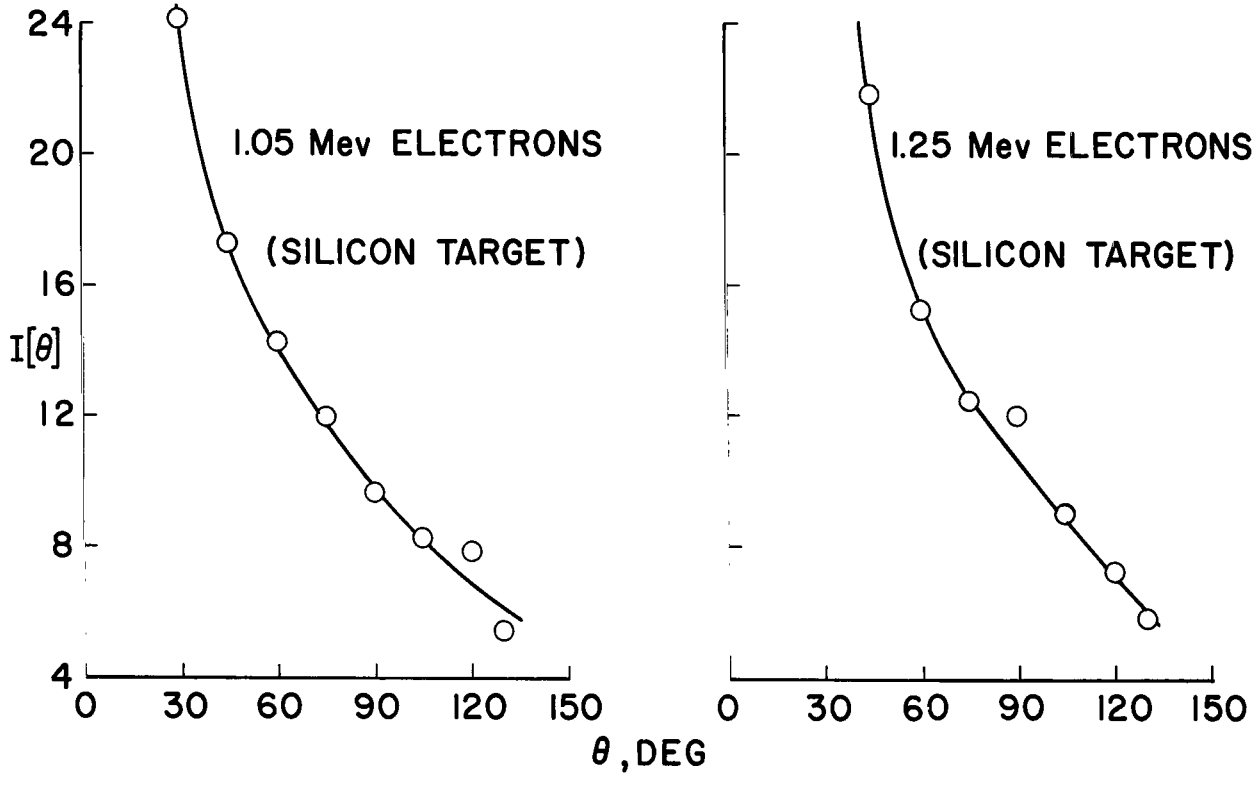

(a) Silicon at 1.05 MeV.

(b) Silicon at 1.25 MeV.

Figure 8.- Angular distribution of total radiated energy.

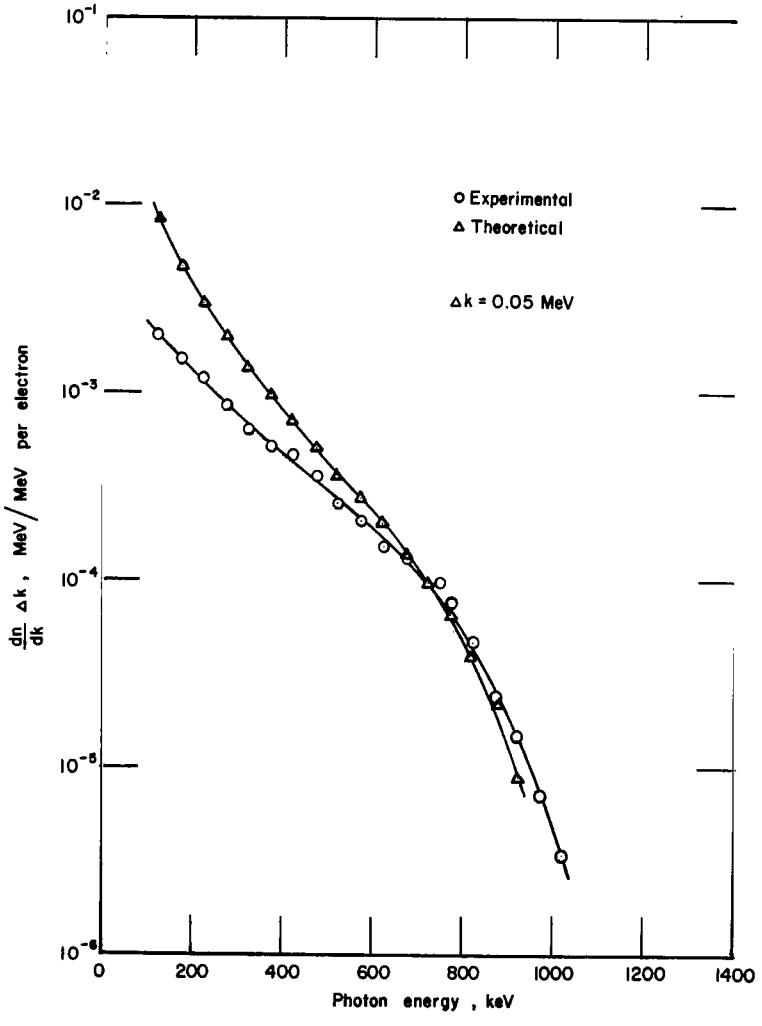

(a) 1.05 MeV electron energy.

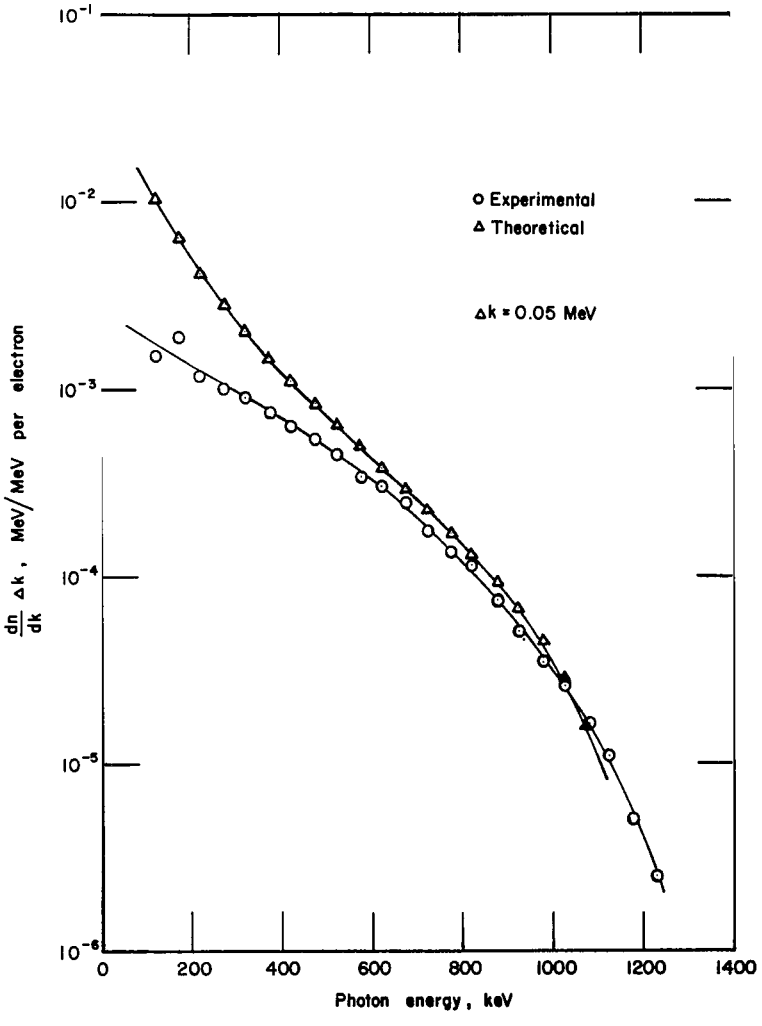

(b) 1.25 Mev electron energy.

Figure 9.- Variation of dn/dk with k in silicon.

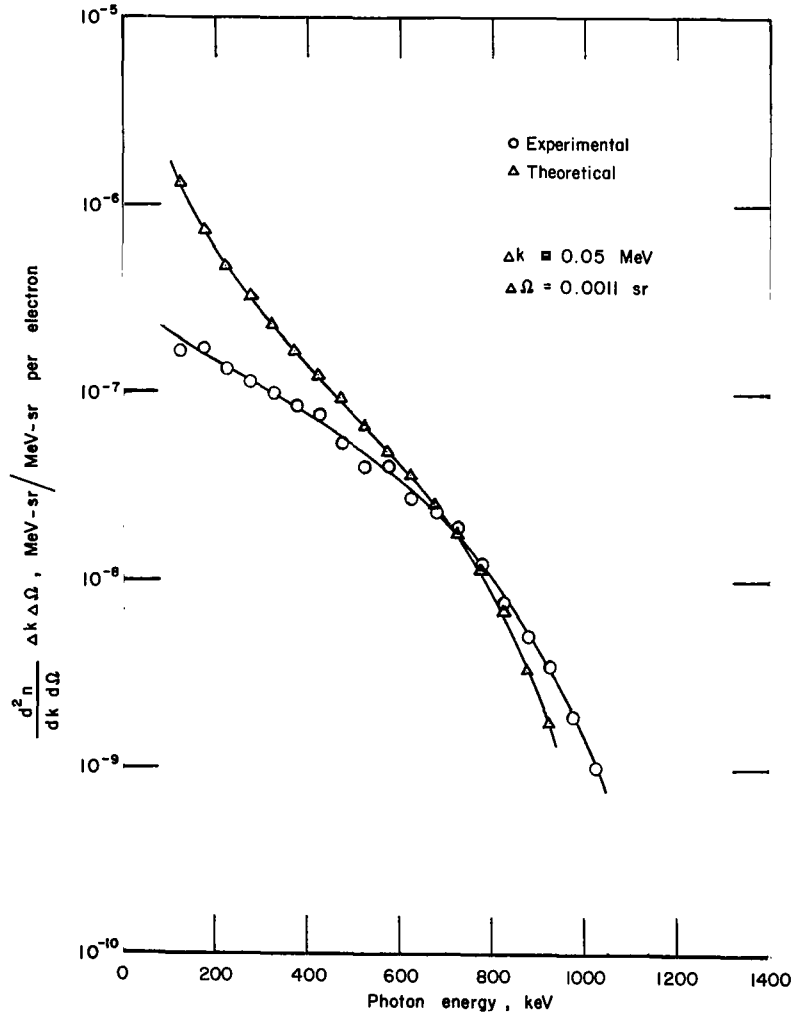

(a) 1.05 MeV electron energy.

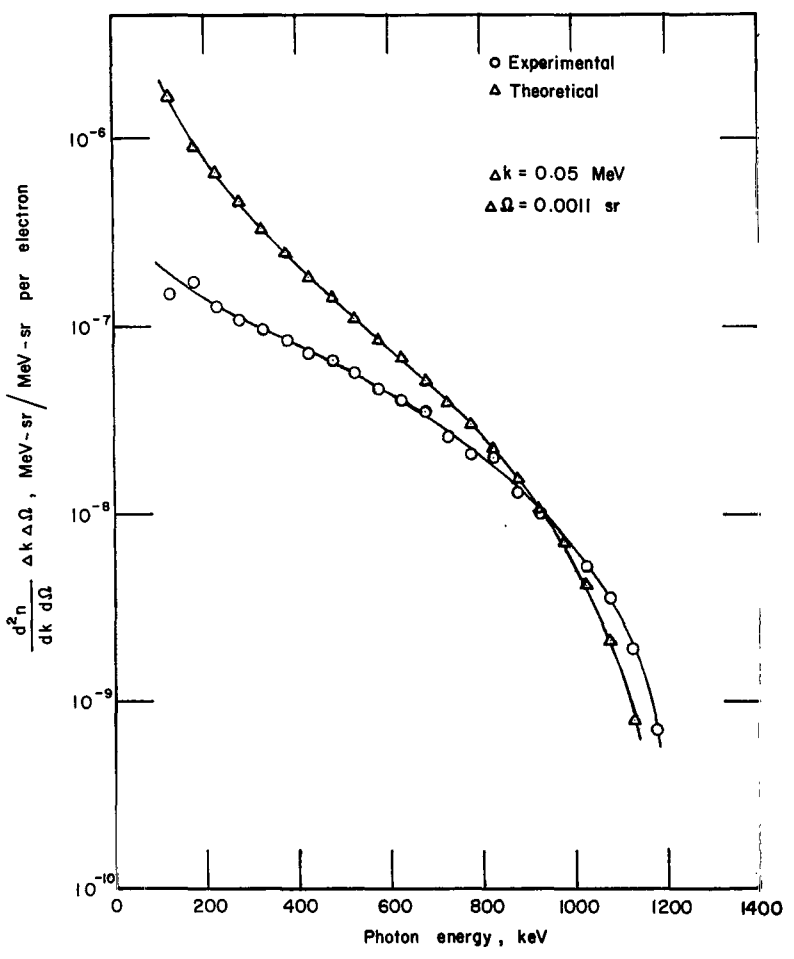

(b) 1.25 MeV electron energy.

Figure 10.- Variation of $d^2n/dk\,d\Omega$ with k at $\theta = 45^\circ$ in silicon.

2/22/85

"The aeronautical and space activities of the United States shall be conducted so as to contribute . . . to the expansion of human knowledge of phenomena in the atmosphere and space. The Administration shall provide for the widest practicable and appropriate dissemination of information concerning its activities and the results thereof."

—NATIONAL AERONAUTICS AND SPACE ACT OF 1958

NASA SCIENTIFIC AND TECHNICAL PUBLICATIONS

TECHNICAL REPORTS: Scientific and technical information considered important, complete, and a lasting contribution to existing knowledge.

TECHNICAL NOTES: Information less broad in scope but nevertheless of importance as a contribution to existing knowledge.

TECHNICAL MEMORANDUMS: Information receiving limited distribution because of preliminary data, security classification, or other reasons.

CONTRACTOR REPORTS: Technical information generated in connection with a NASA contract or grant and released under NASA auspices.

TECHNICAL TRANSLATIONS: Information published in a foreign language considered to merit NASA distribution in English.

TECHNICAL REPRINTS: Information derived from NASA activities and initially published in the form of journal articles.

SPECIAL PUBLICATIONS: Information derived from or of value to NASA activities but not necessarily reporting the results of individual NASA-programmed scientific efforts. Publications include conference proceedings, monographs, data compilations, handbooks, sourcebooks, and special bibliographies.

Details on the availability of these publications may be obtained from:

SCIENTIFIC AND TECHNICAL INFORMATION DIVISION

NATIONAL AERONAUTICS AND SPACE ADMINISTRATION

Washington, D.C. 20546